Mobility and intrinsic performance of silicon-based Nanosheet FETs at 3nm CMOS and beyond

A. Dixit, A. Rezaei, N. Xeni, N. Kumar, T. Dutta, I. Topaloglu, P. Aleksandrov, V. Georgiev, and A. Asenov
James Watt School of Engineering, University of Glasgow, Glasgow G12 8QQ, UK.

***Abstract*—Nanosheet Field-Effect Transistors (NSFETs) have been introduced in the 3nm CMOS technology due to advantages over the FinFET technology. In this paper, using our in-house NanoElectronics Simulation Software (NESS), we explore the mobility and the intrinsic performance of NSFETs for different channel orientations. The effective masses for different cross-sections and channel orientations are extracted from the first principal simulations. The mobility and the intrinsic performance will be evaluated using the effective mass based on the non-equilibrium Green's function (NEGF) and Kubo-Greenwood simulation engines of NESS. The proposed work provides insight into the optimised parameters for NSFET configurations suitable for 3nm and further technology nodes.**

***Keyword-component*—Nanosheet, field-effect transistors, NSFET, NEGF, QuantumATK, first principle, NESS**

I. Introduction

NSFETs have been already adopted in the 3nm CMOS technology and show potential for 2nm CMOS and beyond. The nanometer thickness of NSFET is more easily achievable if compared to FinFETs due to the planar orientation of the channel comparing to the vertical orientation in FinFETs [1]. However, the reduction of the NSFET thickness and cross section dimension changes the key physical parameters of the bulk values that require multi-subband transport in order to accurately capture the device performance.

The crystallographic orientation of channel material can significantly impact the electronic and transport properties of NSFETs [2], [3]. NSFETs with [100] channel orientation show excellent device performance, in comparison to [110] and [111] channel orientation. This is due to the symmetry of the crystal structure, which allows for better alignment of the atoms, leading to better charge transport and current. NSFETs with [110] orientation have higher electron mobility than those with [100] due to their anisotropic crystal structure. The [111] orientation is the least commonly used crystal orientation in NSFETs due to its high surface energy, which makes it difficult to growth. However, all of these NSFETs are gate-all-around architectures and anysurface defects on the channel can result in fluctuation of the leakage current and on/off ratios.

The cross-sectional size of NSFET is another key factor that also significantly impacts its performance [4]. As the cross-sectional size decreases, the transistor's dimensions approach the quantum confinement limits, which impacts the electronic properties of the channel material. A smaller cross-sectional size leads to a higher surface-to-volume ratio, which increases surface effects, and, as a result, decreases the mobility resulting in poor device electrical characteristics [5]. Therefore, understanding the effect of different cross-section sizes on the performance of NSFETs is crucial.

II. Results and Discussions

The cross-sections of devices simulated in this work are illustrated in Fig. 1(a). They represent the 3nm CMOS technology, with a channel cross-section of 3×12nm and 1nm oxide thickness surrounding it. In this study we consider only n-channel transistors although NESS has also a p-channel NEGF engine. The NESS Structure Generator (SG) can introduce the common sources of statistical variability. Here, we have applied Surface Roughness (SR) at the channel/oxide interface as shown in Fig. 1(b), which will be used when the effects of surface roughness and confinement fluctuation scattering are investigated.

Transport is carried out with the electron effective mass NEGF transport module of (NESS) [6]. The simulation flow starts with the first principle band structure simulations using QuantumATK for various cross-sections and channel orientations as shown in Fig. 1(c). The Effective Mass Extractor (EME) module included in NESS is used to extract the transport and confinement effective masses by using parabolic band approximation with the correct minima extracted from the sub-band dispersion relations. Accordingly, the effective masses for each orientation, for multiple cross-sections, from 3×3nm up to 3×12nm, are shown in table I.

In Fig. 2, we have shown that our parabolic approximation is in agreement with the minima of the conduction band for all three orientations and for both the 3×3nm and 3x12 nm cross-sections. Table II represents the deformation potentials and energies for intra- and inter-valley transitions within the optical scattering mechanism. Moreover, utilising the aforementioned values, in fig 3, we present the ballistic, e-ph (PH) and PH+SR scattering I_D-V_G characteristics of two types of device cross-section, i.e., strong confinement (3x3nm) and bulk-like masses (3x12nm). Based on our results we can conclude that for all devices the drive current (Ion) is higher for ballistic as compared to other scattering mechanisms. Also, there is a minimal difference in the leakage current (Ioff) for all orientations. Consistently with the physics and theory both Ion and Ioff current increase with the increment in the cross-section dimension with a slight decrement in Ion/Ioff ratio due to the loss of the electrostatic gate control. In summary, our work shows that NSFET with [110] crystal orientation and 3x3nm cross-section performs the best in comparison to [100] and [111] devices both at low and high drain bias. This is due to the variation in effective mass for the z-valley along the y-direction that increases the possible recombination with asymmetry between the y and z-directions.

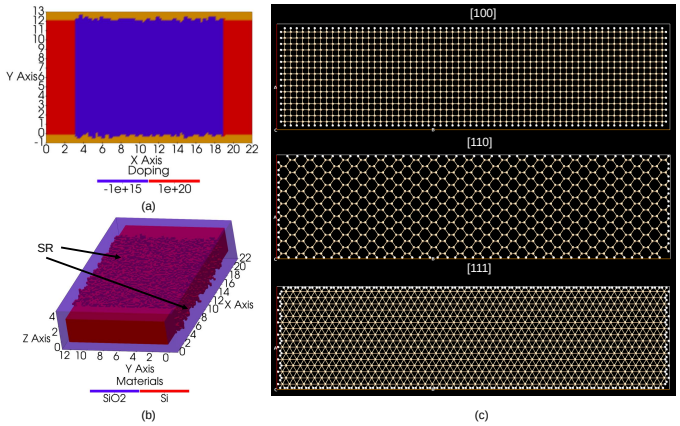

Fig. 1. (a) The SG 2D representation of the doping profile of the 3×12nm NS, cross-section of the z-axis along the channel. (b) The SG 3D representation of the 3×12nm NSFET section showing the Surface Roughness of the channel. (c) The crystalline cross-section from QATK for orientations [100] (top), [110] (middle), and [111] (bottom).

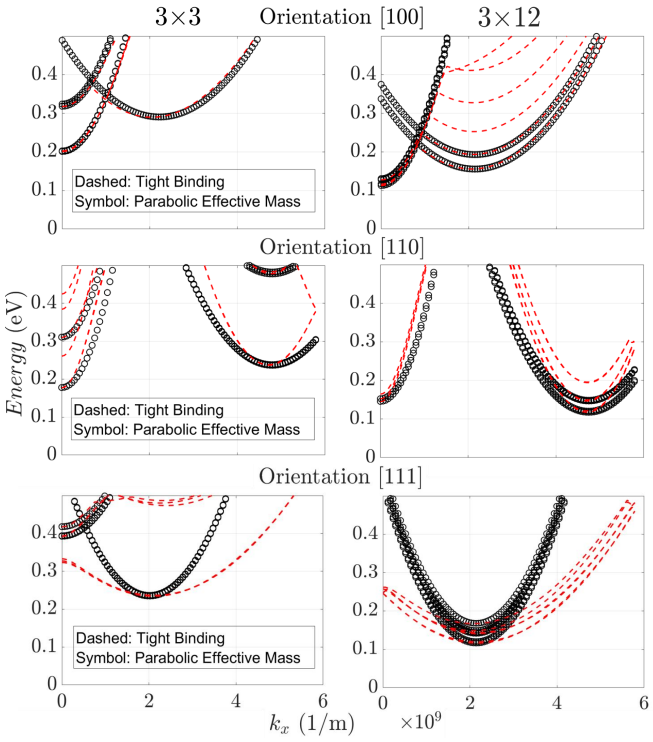

Fig. 2. Comparison of the low conduction band minima of the QATK TB and the Parabolic approximation from NESS for cross-sections 3×3nm and 3×12nm – orientations [100] (top), [110] (middle) and [111] (bottom).

TABLE I

Extracted effective masses from the EME module of NESS for orientations [100], [110], [111] across four different cross-sections with 3nm height.

		[100]			[110]			[111]		
Width [nm]	Valley	m_y [m_0]	m_z [m_0]	m_x [m_0]	m_y [m_0]	m_z [m_0]	m_x [m_0]	m_y [m_0]	m_z [m_0]	m_x [m_0]
3	Δ_x	0.278	0.278	0.945	0.496	0.259	0.568	0.763	0.22	0.455
	Δ_y	1.03	0.251	0.271	0.489	0.258	0.568	0.765	0.218	0.455
	Δ_z	0.251	0.993	0.271	0.303	0.908	0.164	0.229	0.661	0.455
6	Δ_x	0.239	0.273	0.935	0.257	0.374	0.509	0.316	0.371	0.428
	Δ_y	0.524	0.372	0.24	0.263	0.361	0.509	0.32	0.356	0.428
	Δ_z	0.544	0.36	0.24	0.955	0.28	0.159	0.417	0.28	0.428
9	Δ_x	0.478	0.281	0.954	0.587	0.375	0.526	1.116	0.383	0.426
	Δ_y	1.167	0.375	0.239	0.61	0.363	0.526	1.089	0.368	0.426
	Δ_z	1.274	0.36	0.239	2.303	0.284	0.169	1.189	0.307	0.426
12	Δ_x	0.206	0.281	0.959	0.265	0.377	0.518	0.279	0.378	0.427
	Δ_y	0.525	0.375	0.236	0.274	0.364	0.518	0.268	0.366	0.427
	Δ_z	0.592	0362	0.236	1.049	0.281	0.171	0.295	0.303	0.427

TABLE II

Deformation potentials and energies considered for different branches in the optical scattering mechanism. The D_P for acoustic phonon is set to 14.5eV.

Optical Phonon Type	D_P (eV/m)	Energy (eV)
g-type, TA	5×10^9	0.012
g-type, LA	8×10^9	0.0185
g-type, LO	11×10^{10}	0.063
f-type, TA	3×10^9	0.0189
f-type, LA	2×10^{10}	0.0474
f-type, TO	2×10^{10}	0.059

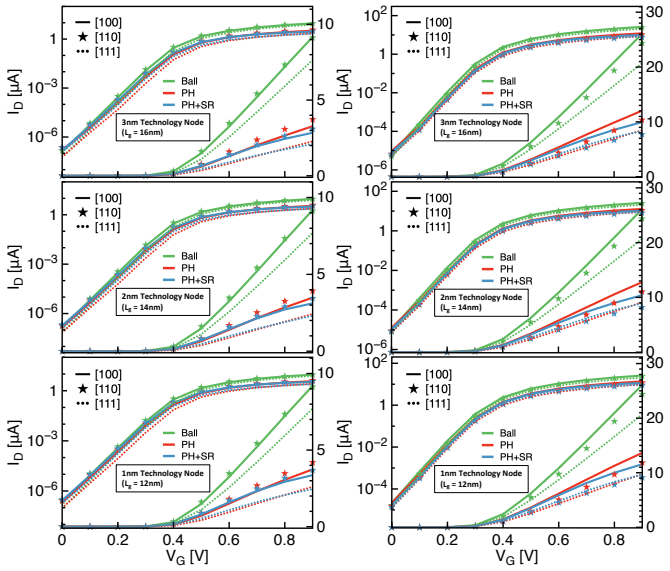

Fig. 3. 3nm and beyond (top to bottom) I_D-V_G characteristics at V_D = 0.05V for (left panel) 3×3nm and (right panel) 3×12nm cross-section. PH represents the combined optical and acoustic scattering processes. Δ_{rms} and correlation length for SR scattering are set to 0.4 and 1.3nm, respectively.

REFERENCES

[1] Veloso, A., *et al*., 2019. "Vertical nanowire and nanosheet FETs: device features, novel schemes for improved process control and enhanced mobility, potential for faster & more energy efficient circuits." In 2019 IEEE International Electron Devices Meeting (IEDM) (pp. 11-1). IEEE.

[2] Niquet, Y.M., *et al*., 2006. "Electronic structure of semiconductor nanowires." Physical Review B, 73(16), p.165319.

[3] Zhang, S., Huang, J.Z., *et al*., 2019. "Design considerations for Si-and Ge-stacked nanosheet pMOSFETs based on quantum transport simulations." IEEE Transactions on Electron Devices, 67(1), pp.26-32.

[4] Jang, D., *et al*., 2017. "Device exploration of nanosheet transistors for sub-7-nm technology node." IEEE Transactions on Electron Devices, 64(6), pp.2707-2713.

[5] P. Ye, T. Ernst and M. V. Khare, "The last silicon transistor: Nanosheet devices could be the final evolutionary step for Moore's Law," in IEEE Spectrum, vol. 56, no. 8, pp. 30-35, Aug. 2019.

[6] S. Berrada, *et al*., "Nano-Electronic Simulation Software (NESS): A Flexible Nano-device Simulation platform," J. Comput. Electron. 19, 1031-1046, (2020).